Article

Journal of Vibration and Control
0(0) 1–12

DOI: 10.1177/1077546313500367
jvc.sagepub.com

Sensorless anti-swing control for overhead crane using voltage and current measurements

Amin Gholabi[1], Mohammad Ebrahimi[1], Gholam Reza Yousefi[1], Mostafa Ghayour[2], Ali Ebrahimi[2] and Hamed Jali[1]

Abstract

One of the most critical issues in overhead cranes is the swing of a suspended load while the crane starts to move and accelerates, changes the movement direction, breaks or stops. This can lead to severe damage, and therefore several methods have been applied to damp the load swings. Most of these methods are based on information about the swing angle of a suspended load. In traditional methods, camera vision, acceleration or inclinometers sensors, simple pendulums and other types of sensors have been used. Generally, a method is desired if it can estimate the swing angle with the least equipment costs, while using an uncomplicated calculation method and the minimum sensitivity to environmental situations and industrial noises. In this paper, a new algorithm is proposed to estimate the swing angle. To do so, the supplied voltage and current of the induction motor which drives the trolley are measured, and then using a new proposed method based on a dynamic analysis of the mathematical dynamic model, the swing angle is estimated and is used in the controller system to damp the swings. The proposed method is verified by means of computer simulations.

Keywords

Anti-swing, overhead crane, sensorless, swing angle estimation, trolley

1. Introduction

Nowadays overhead cranes are used widely in industrial workshops, factories and transport terminals. An overhead crane consists of a trolley, bridge and hoist. A suspended load could swing when a direction or speed change command applies to the trolley (or bridge) or when wind force or any other external factor has impact on the crane operation. These swings may cause human danger, equipment damage, and the position control accuracy could be affected.Therefore, it should be suppressed as much as possible (Trabia et al., 2008).

In order to control the swing angle in cranes, different methods are discussed in the literature and so many researches have been carried out over recent years (Abel-Rahman et al., 2003). Generally, those methods could be categorized into open loop and closed loop methods. The earliest methods of open load swing control were based on optimal time control. Noakes and Jansen (1992) presented an open loop control method based on the relationship between trolley acceleration and payload oscillation, and they showed that the oscillation can be damped by means of programmed acceleration profiles. Park et al. (2000) optimized the load swing controller performance by a combination of input signal shaping technique and a time-efficient feedback control. Garrido et al. (2008) optimized the input shaping technique by means of an extra signal that combines with input; it makes the system robust against the external sway. As far as all the mentioned methods are based on open loop control, the system could experience severe swings when an unforeseen disturbance occurs.

Closed loop control is used in the second group. In these methods, the amount of the swing angle

[1]Department of Electrical and Computer Engineering, Isfahan University of Technology, Isfahan, Iran
[2]Department of Mechanical Engineering, Isfahan University of Technology, Isfahan, Iran

Received: 14 December 2012; accepted: 29 June 2013

Corresponding author:
Mohammad Ebrahimi, Department of Electrical and Computer Engineering, Isfahan University of Technology, Isfahan, 84156-83111, Iran.
Email: mebrahim@cc.iut.ac.ir

should be known, and the controller could be designed according to the amount of load swing angle, speed and trolley position. In these situations, load swings due to unforeseen disturbances could be damped. The closed loop control systems are implemented using different techniques. For instance, Piazzi and Visioli (2002) proposed an approach that is based on a linearized model of the crane and consists of damping the linearized system by an observer-based controller. Since the complete model of an overhead crane is nonlinear, the major researches have been done on nonlinear controllers of cranes. Ebeid et al. (1992) presented a nonlinear electromechanical model describing the dynamical behavior of overhead cranes. Liu et al. (2004) and Chang (2007) designed an adaptive controller by combining the second order sliding mode and fuzzy controller, and an adaptive fuzzy controller, respectively. The latter does not need the complex dynamic model of the crane system, but it uses trolley position and swing angle information. Park et al. (2008) introduced an adaptive fuzzy sliding-mode control. The main controller includes a path tracking controller, and in order to damp the sways, a fuzzy sliding mode controller has been used.Chwa (2009) proposed a nonlinear tracking control method for a three-dimensional crane that works well when there is an initial swing angle and load weight variation. Solihin et al. (2010) illustrated that proportional-integral-derivative (PID) controllers cannot always effectively control the swings when the parameters of system vary. Then they presented a fuzzy-tuned PID controller to overcome this problem. Pannil et al. (2010) presented a linear quadratic Gaussian optimal control method with an additional weighting function. In this method, the swing angle is controlled smoothly. Yu and Li (2010) introduced a smart fuzzy compensator to compensate the gravity and friction in order to damp the overhead crane sways. Cao and Liu (2011) proposed a method for damping the sway and position control of an overhead crane. In this technique, an indirect adaptive fuzzy sliding mode controller is used and uncertainties of load mass are considered. Tsai et al. (2011) have modeled an overhead crane system as a low-order linearized plant, so they reduced the complexity of synthesis of feedback controllers. Deng et al. (2012) proposed a robust nonlinear controller, for displacement control of the trolley and the swing angle. They have used a generalized Gaussian function and robust right coprime factorization approach. Saeidi et al. (2012) presented a neural network self-tuner (NNST) controller in order to move the load precisely, as well as to eliminate its sway.

In the entire abovementioned closed loop methods, the load swing angle should necessarily be obtained in order to damp the swings. Usually, a camera and a microprocessor-based system are used to obtain the load swing angle, such as Siemens (1999), Sorensen (2005) and Sano et al. (2012). It should be mentioned that the camera could be installed under the trolley and near the rope holder point. Therefore, the main disadvantages of these methods include cost consumption and lower operation precision when there is pollution in industrial environments or when it is raining in open door environments. As an example, Kaneko et al. (2009) illustrated that utilization of a vision system in the sway angle detection could result in the deterioration of the control performance owing to the influence of weather as well as delay in detection. Therefore, in recent years, load swing angle estimation using variables that are available or could be easily measured by low price sensors has been considered. For example, Rushmer et al. (1995) used a simple pendulum to estimate the velocity and displacement of the suspended load. In addition Kim et al. (2001) have proposed a new vision-sensorless anti-sway control scheme, where the sway angle of the load is estimated with a simple acceleration sensor which can be installed on the trolley. Also Kim et al. (2004), used inclinometers as an equipment to determine the swing angle.

Solihin (2009) has designed a dynamic recurrent neural network (DRNN) based soft sensor instead of the real swing angle sensor. The DRNN is trained using input-output data to estimate the payload swing angle from trolley acceleration and input voltage of the trolley actuator. Wen et al. (2011) proposed an operator-based robust nonlinear control for a crane system, in which the angle of the swing cable is estimated by using Support Vector Machine (SVM)-based model. Ebrahimi et al. (2011) measured forces using installed vertical and horizontal load cells aimed to estimate the swing angle. Deng et al. (2012) have estimated the swing angle of a payload, by means of data-based support vector regression to deal with the uncertainty and dynamics of a crane system which are not modeled.

Zhong and Zhan (2012) have deduced the swing angle via dynamic equations analysis obtaining a transfer function between the load angle and the force acting on the trolley.

Nevertheless, researches about load swing angle estimation have been continued and the goal is price reduction and using simple methods which are not based on complicated mathematical models, have sufficient precision and are insensitive with respect to environmental situations.

In this paper, a new method for suspended load swing angle estimation in overhead cranes is introduced. This method is based on measuring the voltage and current of trolley drive motor.

This paper is organized as follows. In Sections 2, and 3, the system structure and system modeling are described, respectively. The swing angle estimator

system (i.e. anti-swing controller) is the subject of Section 4. Simulation results and conductions are brought in Sections 5 and 6, respectively.

2. Description of the structure and operation of the overhead cranes and the load swing phenomena

The basic parts of an overhead crane, as shown in Figure 1, are: trolley, bridge, hoist, suspended load, electrical motor(s) and the operator's cabin. In this system, the axis of the wheel connects to the motor shaft through a gear box, and an electrical torque drives the wheel on the rail. This rotation is associated with a slip which converts the electrical torque to the adhesive force (F_{ad}) on the wheel rim, and due to this force the trolley moves (Umez-Eronini, 1998). The reaction of the adhesive force will also apply to the electrical motor as the load torque.

A three-phase squirrel cage induction motor has been used as the actuator for the trolley. According to the advantages of the vector control, this method is used to control the crane drive. In this method, produced electrical torque follows the reference torque, over the transient and steady state situations (Vas, 1998).

Another important issue in the overhead cranes is the suspended load swing phenomena. The physical explanation of this phenomenon is as follows.

It is assumed that when the trolley (or bridge) starts to move, the rope connected to the suspended load is in the vertical position and the applied horizontal force to the load is zero. When the trolley moves, the load will be pulled. Therefore, the rope will have a negative angle with respect to the vertical line (θ). This angle is called the swing angle. When this angle exists, a horizontal force is applied to the suspended load and causes acceleration in the load. When the trolley moves, if θ is not controlled, the load could oscillate. This phenomenon is called swing. The same phenomenon occurs over speed reduction, breaking and stopping periods, and also when the direction and/or speed changes (Ebrahimi et al., 2011).

It is important to control and damp the suspended load swing and control the position of the load, in order to prevent human danger and to avoid financial losses. To do so, in most kinds of controller systems, the precise amount of θ is required, and thus has to be measured or estimated.

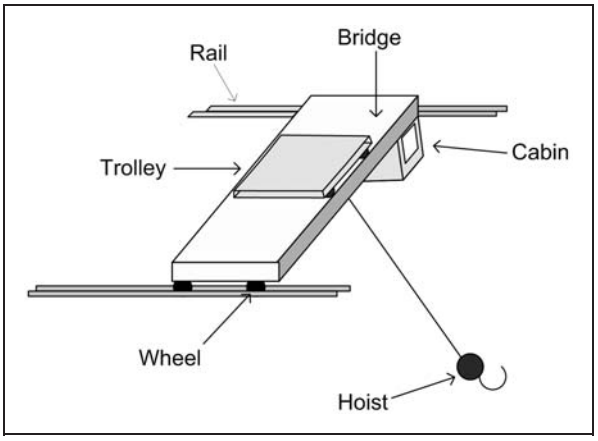

Figure 1. Overhead crane structure.

3. Swing angle estimator using voltage and current signals

In this section, a new method for estimating the load swing angle is introduced. This method does not need any camera and image processing system or any mechanical sensor. The proposed method is based on mathematic dynamic model analysis of the trolley and suspended load movement, wheel and rail equation, as well as induction motor drive equations. To perform this analysis, first, analytic equations which define the relation between the trolley forward driven force accelerator force and load swing are extracted. Then, the relation between this force and the electrical torque and speed of motor rotation is formulated. The electrical torque and speed of the induction motor could be estimated using measured voltage and current of the motor. Based on this fact, the block diagram of load swing angle estimator is designed. Input signals of this estimator include the measured voltage and current of trolley motor drive, and its output is the suspended load swing angle.

3.1. Derivation the relation between load swing angle and forward dive force

A suspended load has a swing movement and this leads to the application of a variable force to the junction which connects the rope to the trolley. This force is the rope tension and will be denoted by T. According to Figure 2, T has two components as T_x and T_y (Ebeid et al., 1992).

The suspended load has a relative acceleration with two components, one component is tangent to the load swing path $a_{mt} = l\ddot{\theta}$, and the other component is perpendicular to the swing movement path $a_{mn} = l\dot{\theta}^2$. With mapping acceleration components on Y axis, a_{my} will be obtained as:

$$a_{my} = l\dot{\theta}^2 \cos\theta + l\ddot{\theta} \sin\theta \quad (1)$$

The motion equations of load in the Y and X directions are:

$$T_y = mg + ml(\dot{\theta}^2 \cos\theta + \ddot{\theta}\sin\theta) \tag{2}$$

$$T_x = T_y \tan\theta = mg\tan\theta + ml(\dot{\theta}^2 + \ddot{\theta}\tan\theta)\sin\theta \tag{3}$$

Applying Newton's second law for the trolley and suspended load in X-axis direction will result in equations (4) and (5), respectively:

$$F_{ad} + T_x = F_{ad} + [mg\tan\theta + ml(\dot{\theta}^2 + \ddot{\theta}\tan\theta)\sin\theta] = M_t\ddot{x} \tag{4}$$

$$-[mg\tan\theta + ml(\dot{\theta}^2 + \ddot{\theta}\tan\theta)\sin\theta] = m\ddot{x}_m \tag{5}$$

If equations (4) and (5) are multiplied by $\frac{1}{M_t l}$ and $\frac{1}{ml}$, respectively, then equation (4) is subtracted from equation (5), there can be written:

$$\frac{F_{ad}}{M_t l} = -\frac{m+M_t}{M_t l} g\tan\theta - \frac{m+M_t}{M_t} \times (\dot{\theta}^2 + \ddot{\theta}\tan\theta)\sin\theta + \frac{\ddot{x} - \ddot{x}_m}{l} \tag{6}$$

According to Figure 2, it can be seen that $\sin\theta = (x_m - x)/l$, and considering a constant length for the rope while trolley is moving, and by two times differentiation of $\sin\theta$ the result will be:

$$\frac{d^2}{dt^2}\sin\theta = \frac{\ddot{x}_m - \ddot{x}}{l} \tag{7}$$

Substituting equation (7) in equation (6) yields:

$$\frac{F_{ad}}{M_t l} = -\frac{m+M_t}{M_t l}\cdot g\cdot\tan\theta - \frac{m+M_t}{M_t} \times (\dot{\theta}^2 + \ddot{\theta}\tan\theta)\cdot\sin\theta - \frac{d^2}{dt^2}\sin\theta \tag{8}$$

As it is shown in equation (8), the forward driving force of the trolley is expressed as a single variable function of the swing angle. Thus, if the amount of the forward driving force is known, the amount of the swing angle can be determined, at every instant of time.

3.2. Forward driving force estimation

As mentioned in Section 2, the trolley's forward drive force is equal to adhesive force (F_{ad}) on the wheel rim (Figure 3). Therefore, the amount of the load torque entered on the trolley's motor is proportional to the forward drive force, as formulated in equation (9),

$$F_{ad} = \frac{T_l}{\alpha r} \tag{9}$$

in which T_l is motor load torque, α is gearbox coefficient, and r is radius of the trolley's wheel.

According to the rotational movement of the motor shaft and connected components to the motor, and with implementing Newton-Euler's law in motor rotation direction, equation (10) will be extracted, in which J is the motor and its connected components moment of inertia, T_e is motor electromagnetic torque, and ω is motor rotation speed.

$$T_e - T_l = J\frac{d\omega}{dt} \tag{10}$$

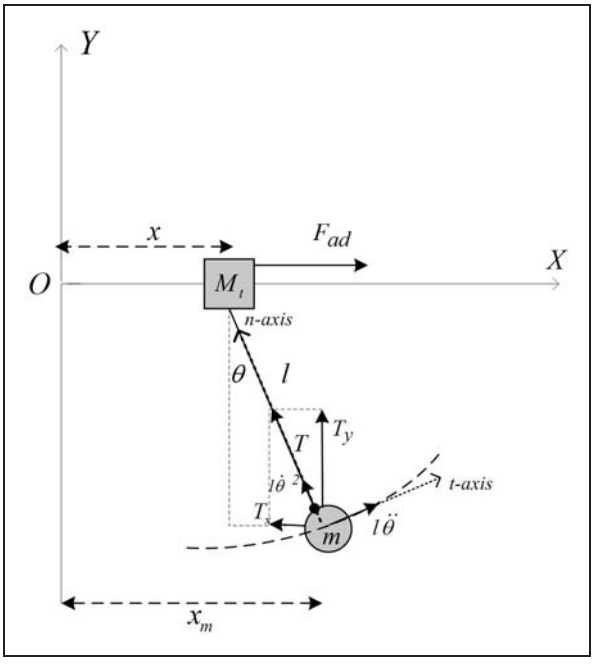

Figure 2. Free-body diagram of trolley and acceleration components of suspended load.

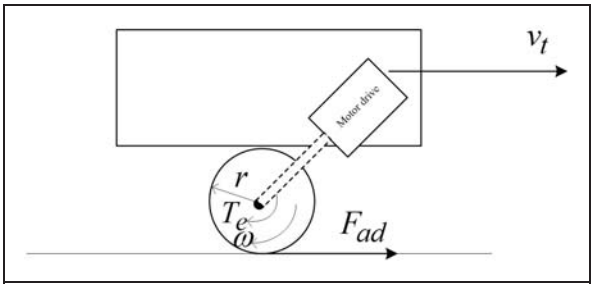

Figure 3. Trolley wheel-rail model.

Combining equations (9) and (10) will result:

$$F_{ad} = \frac{\left(T_e - J\frac{d\omega}{dt}\right)}{\alpha r} \tag{11}$$

Equation (11) shows that if the amount of the motor electric torque and motor rotation speed are known, the amount of forward drive force of the trolley could be estimated at any time.

In the following, a method for estimating the motor electrical torque and motor speed by using measured supplied voltage and the current of the trolley's motor is introduced.

3.3. Electric torque estimation

Different methods have been presented for induction motor electrical torque estimation using measurable variables. As an example, Vas (1998) has used equation (12) to calculate the electrical torque:

$$T_e = -\frac{3}{2}pL_m\left(i_{sD}i_{rq} - i_{sQ}i_{rd}\right) \tag{12}$$

where i_{sD} and i_{sQ} are stator current components, i_{rd} and i_{rq} are rotor current components in a stationary reference frame, respectively. To do so, first stator three-phase current (i_{sA},i_{sB} and i_{sC}) should be measured, and then using below equations, i_{sD} and i_{sQ} will be calculated:

$$i_{sD} = i_{sA} - \frac{1}{2}(i_{sB} + i_{sC}) \tag{13}$$

$$i_{sQ} = \frac{1}{\sqrt{3}}(i_{sB} - i_{sC}) \tag{14}$$

To obtain i_{rd} and i_{rq}, the calculations below should be performed. First, using measured three-phase stator voltages (V_{sA}, V_{sB} and V_{sC}), values of V_{sD} and V_{sQ} will be calculated as:

$$V_{sD} = V_{sA} - \frac{1}{2}(V_{sB} + V_{sC}) \tag{15}$$

$$V_{sQ} = \frac{1}{\sqrt{3}}(V_{sB} - V_{sC}) \tag{16}$$

According to three-phase balanced system, measuring two phase currents and two phase voltages would be sufficient to calculate the third one. Therefore, two current sensors and two voltage sensors would be enough in this drive. Meanwhile, in the normal operation of the inverter, the output voltages would track the reference voltages, accurately. Therefore it would be possible to use reference voltages instead of using sensors to measure the voltages (Vas, 1998).

Values of stator fluxes (ψ_{sD} and ψ_{sQ}) are calculated using stator voltages and current values:

$$\psi_{sD} = \int (V_{sD} - R_s i_{sD})\mathrm{d}t \tag{17}$$

$$\psi_{sD} = \int (V_{sD} - R_s i_{sD})\mathrm{d}t \tag{18}$$

On the other hand, stator fluxes are linear functions of stator voltages and rotor currents, as demonstrated in equations (19) and (20) given by:

$$\psi_{sD} = L_s i_{sD} + L_m i_{rd} \tag{19}$$

$$\psi_{sQ} = L_s i_{sQ} + L_m i_{rq} \tag{20}$$

With combining equations (17) to (20), rotor currents could be obtained with respect to stator voltages and currents, as follows:

$$i_{rd} = \frac{1}{L_m}\int (V_{sD} - R_s i_{sD})\mathrm{d}t - \frac{L_s}{L_m} i_{sD} \tag{21}$$

$$i_{rq} = \frac{1}{L_m}\int \left(V_{sQ} - R_s i_{sQ}\right)\mathrm{d}t - \frac{L_s}{L_m} i_{sQ} \tag{22}$$

With known amount of stator current components (equations (13) and (14)), and rotor current components (equations (21) and (22)), the value of the electrical torque could be estimated (equation (12)).

3.4. Induction motor speed estimation

Speed estimation could be performed with different open loop and close loop methods. In this paper, an open loop method based on dynamic equations is used (Vas, 1998). In a squirrel cage induction motor, the values of rotor voltage components in a stationary reference frame are equal to zero. Therefore, rotor voltage component V_{rq} is as follows:

$$V_{rq} = R_r i_{rq} + \frac{d\psi_{rq}}{\mathrm{d}t} - \omega_r \psi_{rd} = 0 \tag{23}$$

On the other hand, rotor flux components would be:

$$\psi_{rq} = L_r i_{rq} + L_m i_{sQ} \tag{24}$$

$$\psi_{rd} = L_r i_{rd} + L_m i_{sD} \tag{25}$$

By combining equation (23) and (24) and eliminating i_{rq}, the results will be:

$$\omega_r = \frac{1}{\psi_{rd}}\left[\frac{R_r}{L_r}\left(\psi_{rq} - L_m i_{sQ}\right) + \frac{d\psi_{rq}}{\mathrm{d}t}\right] \tag{26}$$

Now, by using equations (21) and (22), and eliminating rotor current components in equations (24) and (25), there can be written:

$$\psi_{rd} = \frac{L_r}{L_m}\int (V_{sD} - R_s i_{sD})\mathrm{d}t - \left(L_m - \frac{L_s L_r}{L_m}\right) i_{sD} \quad (27)$$

$$\psi_{rq} = \frac{L_r}{L_m}\int (V_{sQ} - R_s i_{sQ})\mathrm{d}t - \left(L_m - \frac{L_s L_r}{L_m}\right) i_{sQ} \quad (28)$$

Briefly, to estimate motor speed using measured stator voltages and currents, first using equations (27) and (28), the flux components (ψ_{rd} and ψ_{rs}) are calculated. Moreover, $\frac{d\psi_{rq}}{\mathrm{d}t}$ could be calculated by taking a differentiation from equation (28). Finally, motor speed could be estimated using equation (26).

3.5. Block diagram of swing angle estimator

The swing angle estimator is designed based on dynamic equations of the system. The system block diagram consists of four stages: in the first step, as it is shown in Figure 4, the amount of voltages and currents of the three-phase induction motor are measured and converted to two-phase equivalent voltages and currents using equations (13) to (16). In the second step, by means of the aforementioned voltages and currents and using equations (21) and (22) the values of rotor current components, i_{rd} and i_{rq} are calculated and then according to equation (12) the value of thte electrical torque is estimated. Furthermore, using equations (27) and (28) the rotor flax components, ψ_{rd} and ψ_{rq}, are calculated and the electrical speed is estimated using equation (26).

In the third step, by means of the estimated electrical torque and the electrical speed and equation (11), the value of driving force ($\hat{F}_{ad}$) is estimated. Finally, in the fourth step, using driving force ($\hat{F}_{ad}$) and equation (8), the swing angle ($\hat{\theta}$) is estimated. This estimated angle will be used in the anti-swing controller.

In the following it will be shown that each layer and the overall system in Figure 4 is bounded input bounded output (BIBO) and has limited steady state output error when there is a limited input error.

The convergence of the first layer, speed and torque estimation based on the measured voltage and current, is analyzed and approved in several references such as Vas (1998).Therefore, if Δi_s and Δv_s, the maximum deviations of the measured current and voltage are limited values, then ΔT_e and Δw will be limited as well. Δ denotes a small variation around the operating point of each variable.

Regarding driving force estimator, i.e., the second block in Figure 4, by linearization of equation (11) there can be written:

$$\Delta F_{ad} = \frac{\Delta T_e}{\alpha r} - \frac{J}{\alpha r}\frac{d}{\mathrm{d}t}(\Delta\omega) \quad (29)$$

The speed variation has a continuous function. Therefore $\frac{d}{\mathrm{d}t}(\Delta\omega)$ is bounded. Denoting the maximum error of ΔT_e and $\frac{d}{\mathrm{d}t}(\Delta\omega)$ by ε_1 and $\varepsilon 2$, respectively, the maximum error of ΔF_{ad} will be bounded according to equation (30):

$$\Delta F_{ad} \le \frac{\varepsilon_1}{\alpha r} + \frac{J\varepsilon_2}{\alpha r} \quad (30)$$

In the third layer in Figure 4, i.e., in swing angle estimation, if θ has a small variation around its operating point ($\theta_0 = 0$), then linearization of equation (8) leads to:

$$\begin{aligned}\frac{\Delta F_{ad}}{M_t l} = &-\frac{M_t + m}{M_t l} g\left(\frac{1}{\cos^2\theta_0}\right)\Delta\theta - \frac{M_t + m}{M_t} \\ &\times\left[\left(2\dot{\theta}_0 \sin\theta_0\right)\Delta\theta_0 + \left(\dot{\theta}_0^2\cos\theta_0\right)\Delta\theta\right. \\ &\left. + \tan\theta_0 \sin\theta_0 \Delta\ddot{\theta} + \ddot{\theta}_0\left(\frac{2\cos^2\theta_0\sin\theta_0 + \sin^3\theta_0}{\cos^2\theta_0}\right)\Delta\theta\right] \\ &- \cos\theta_0 \Delta\ddot{\theta}\end{aligned} \quad (31)$$

Considering $\theta_0 = 0$ in equation (31), the result will be:

$$\frac{\Delta F_{ad}}{M_t l} = \left(-\frac{M_t + m}{M_t l} g - \frac{M_t + m}{M_t l}\dot{\theta}_0^2\right)\Delta\theta - \Delta\ddot{\theta} \quad (32)$$

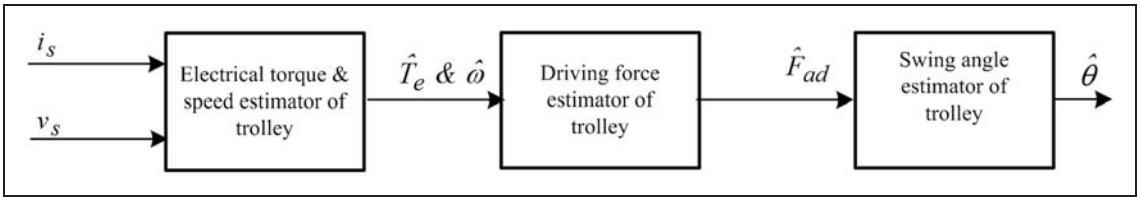

Figure 4. Swing angle estimator block diagram.

Therefore, the transfer function for $\Delta\theta$ would be as follows:

$$\frac{\Delta\theta(s)}{\Delta F_{ad}(s)} = \frac{\frac{-1}{M_t l}}{s^2 + \left(\frac{M_t+m}{M_t l} g + \frac{M_t+m}{M_t}\dot{\theta}_0^2\right)} \tag{33}$$

in which s is the Laplace transform operator. Considering a bounded variation for ΔF_{ad} such as $\Delta F_{ad}(s) = \frac{\Delta F}{s}$, according to the final value theorem, the absolute error of $\Delta\theta$ is given by:

$$|\Delta\theta| \leq \frac{\frac{1}{M_t l}}{\frac{M_t+m}{M_t l} g + \frac{M_t+m}{M_t}\dot{\theta}_0^2} \Delta F \tag{34}$$

Therefore, in the third layer, bounded error in ΔF_{ad} will result in bounded error in $\Delta\theta$.

As it can be seen in Figure 4, there are three decoupled layers of estimators where there is no loading between them. Therefore, bounded error in the input will cause bounded error in the output of the overall estimator.

4. Anti-swing controller

Different methods could be used to control and damp the load swing. In this paper, a proper damping signal is added to the reference speed signal to control and damp the swings (Ebrahimi, et al., 2011). First, trolley and load movement equations are extracted and it will be shown that the system could be modeled by a second order system.

To do so, according to Figure 2, x_m could be written as:

$$x_m = x + l\sin\theta \tag{35}$$

Further, the force equation in tangent direction with the load movement will be as follows:

$$\ddot{x}\cos\theta + l\ddot{\theta} + g\sin\theta = \frac{F_\theta}{m} = 0 \tag{36}$$

where F_θ is proportional to the air friction force (which is small and negligible).

With the assumption that the variation of θ is small and the rope length is fixed, the two abovementioned equations could be restated as:

$$\theta = \frac{x_m - x}{l} \tag{37}$$

$$\ddot{x} + l\ddot{\theta} + g\theta = \frac{F_\theta}{m} = 0 \tag{38}$$

If θ is eliminated between the two abovementioned equations, the result is:

$$\ddot{x}_m + \frac{g}{l} x_m = \frac{g}{l} x \tag{39}$$

After a differentiation, the resulted equation will be as follows:

$$\frac{l}{g}\ddot{v}_m + v_m = v_t \tag{40}$$

According to the fact that $v_t = \dot{x}$ is the real speed of the trolley and $v_m = \dot{x}_m$ is the suspended load speed, the equation which expresses the trolley and load movement is a second order system and does not have the damping term. In order to eliminate load swings, a damping term should be added to the reference speed of the trolley (v_t^*):

$$v_t^{**} = v_t^* - K_d\dot{v}_m \tag{41}$$

where, v_t^{**} is the modified speed reference, $K_d\dot{v}_m$ is damping signal and K_d is the damping coefficient for the second order system (equation (40)).

And also, by combining equation (37) with equation (39), the result would be:

$$\dot{v}_m = \ddot{x}_m = -g\theta \tag{42}$$

Therefore the final form of the modified speed reference could be written as follows:

$$v_t^{**} = v_t^* + K_d g\theta \tag{43}$$

4.1. Block diagram of anti-swing and speed controller

Figure 5 shows a general block diagram for an overhead crane, which consists of a speed controller and suspended load swing damper system.

As it is shown in the block diagram, at first, the trolleys reference speed signals are added to the swing damper signal, the result is compared with the actual trolley's speed and the resulting error fed to a speed controller. The output of this controller makes the reference torque.

This reference torque is applied to the induction motor drive and the motor will produce the desired torque and enters it to the trolley's wheels. Due to the drive force (F_{ad}) applied to the body of the trolley, the system will move with a velocity denoted by v_t, and the suspended load will have a swing, which is denoted by angle θ.

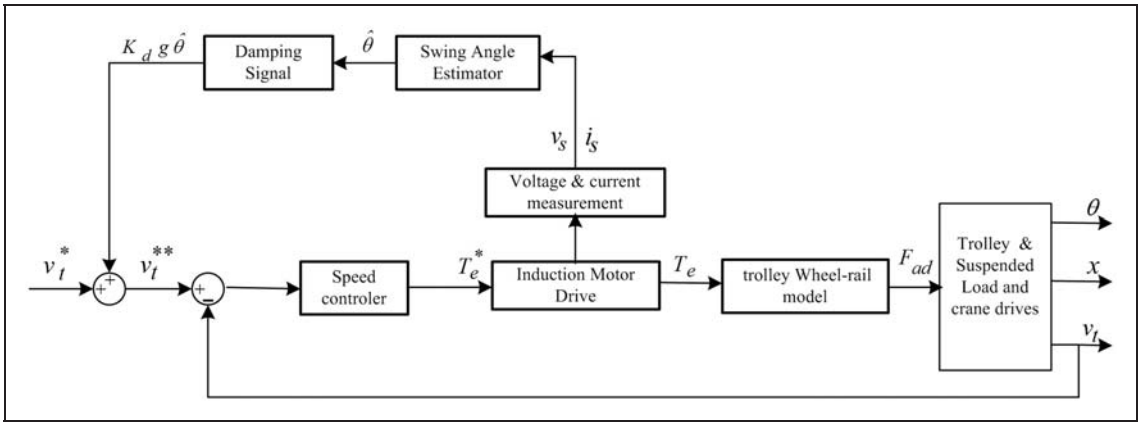

Figure 5. Block diagram of speed control and load's damping swing system.

In this system by measuring the supply voltages and currents of the three-phase induction motor, and according to the proposed system, the amount of swing angle θ will be estimated.In the following, θ will be used to produce a damping signal and will be applied to the control system as described earlier.

5. Simulation of trolley drive with anti-swing controller

A complete set of a trolley and its drive (consisting of body, suspended load that moves on the rails by the wheels, and an induction motor drive in vector control mode) has been considered. The simulation is carried out by means of related equations, and the parameters of a 1 ton overhead crane and a 10 HP induction motor. All the data are reported in Notation (crane parameters).

In order to obtain a complete model of this system, three modeling stages are performed as follows:

- Modeling of wheel movement on the rail considering mechanical slip of the wheel (Ebrahimi, 2011).
- Modeling of the x-axis movement of the trolley and swing of the suspended load. The Lagrangian equation has been used to extract governing roles on the system (Ebrahimi, 2011).
- Modeling of the vector controlled induction motor drive. Two-axis, fifth order model has been used here (Vas, 1998).

The input signal to the controller system is reference trolley's speed (v_t^*) and swing damping signal ($K_d g\theta$). The value of K_d is considered equal to 1.0. The output of the trolley's drive is displacement (x), speed (v_t) and the swing angle (θ).

Moreover, the swing angle estimator is simulated. The required data for this block are the measured voltage and current of the induction motor supply. Matlab-Simulink has been used for the simulations.

5.1. Simulation results

Simulation results are analyzed in two cases as follows:

5.1.1. Case A: speed control scheme without anti-swing regulator. In this case, the system is analyzed in speed control mode without using the anti-swing system where it is verified that the estimated swing angle ($\hat{\theta}$) is compatible with the actual value of the swing angle (θ). Figure 6(a) shows trolley reference speed ($v_t^* =$ solid line), and the actual trolley's speed ($v_t =$ dashed line). As can be seen, to show the drive performance when acceleration and speed are increased, the reference speed is increased with a proper ramp rate, from zero to 0.7 m/s in the first step and then to 1.5 m/s. Further, in order to show the system performance when the direction is reversed, the amount of the reference speed is changed to -1 m/s, and finally to show the performance in break and stop situation, the reference speed is turned to 0.0 m/s.

In Figure 6(b) the amount of the estimated motor speed (ω) in the aforementioned situation is represented. Estimated electrical torque, estimated forward drive force, actual swing angle and estimated swing angle are shown in Figures 6(c) to 6(f), respectively. As can be seen, the estimated swing angle tracks the actual swing angle, properly.

5.1.2. Case B: speed control scheme with anti-swing regulator. In this case, the system is analyzed in speed and control mode using the anti-swing system where the performance of the system in estimating and damping the swing angle over the different situations is presented. Figure 7 shows the system's performance over the situations mentioned in the previous case.

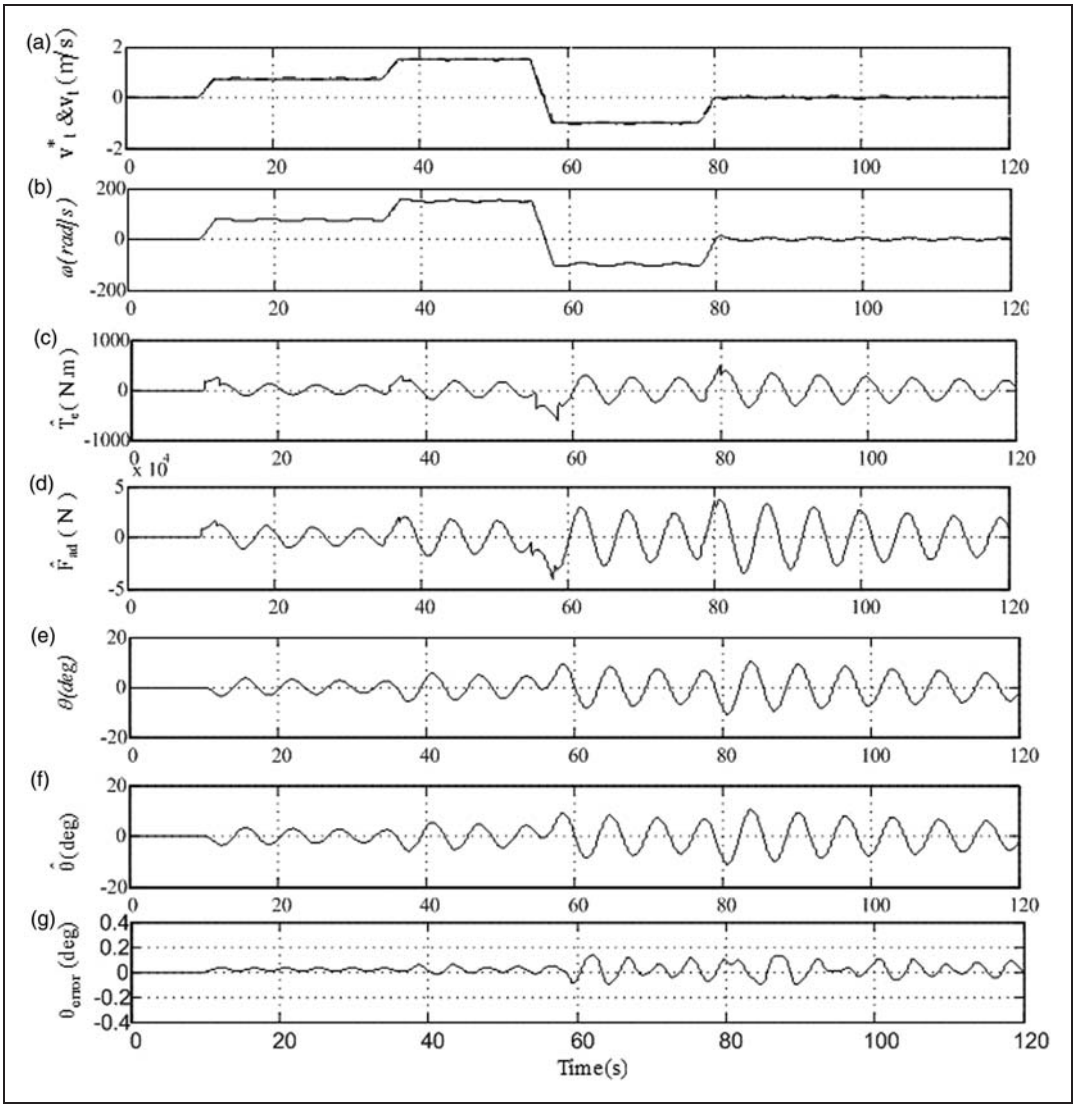

Figure 6. Performance of swing angle estimator without anti-swing regulator (a) Trolley reference speed (solid line), and actual trolley's speed (dashed line), (b) Estimated motor speed, (c) Estimated electrical torque, (d) Estimated forward drive force, (e) Actual swing angle, (f) Estimated swing angle, and (g) Estimation error of swing angle.

In Figure 7(a), the reference speed in an accelerating situation while speed is increasing, reversing movement direction and speed, and also breaking and stop situations are shown. The modified reference speed (v_t^{**}) is illustrated in Figure 7(b). The estimated motor speed, the estimated electrical torque and the estimated forward drive force are illustrated in Figure 7(c) to (e), respectively.

The swing angle has been shown in Figure 7(f) where it could be seen that in this case, due to the desired performance of the swing angle estimator block and the swing damper system, the swing angle has been damped, properly.

It should be mentioned that there is some quasi-swing behavior over the accelerating, changing the direction and breaking moments, due to load mass inertia, which is not considered as swing.

A sensitivity analysis is performed on the plant's parameters in order to study the robustness of the method. The results show that the estimations will converge while there is up to 10% deviation in the parameters. In these situations, the plant is stable and the performance is acceptable. The authors are working on the compensation method when there are more parameter variations.

6. Conclusions

In this paper, a method for estimating the suspended load swing angle in overhead cranes based on the

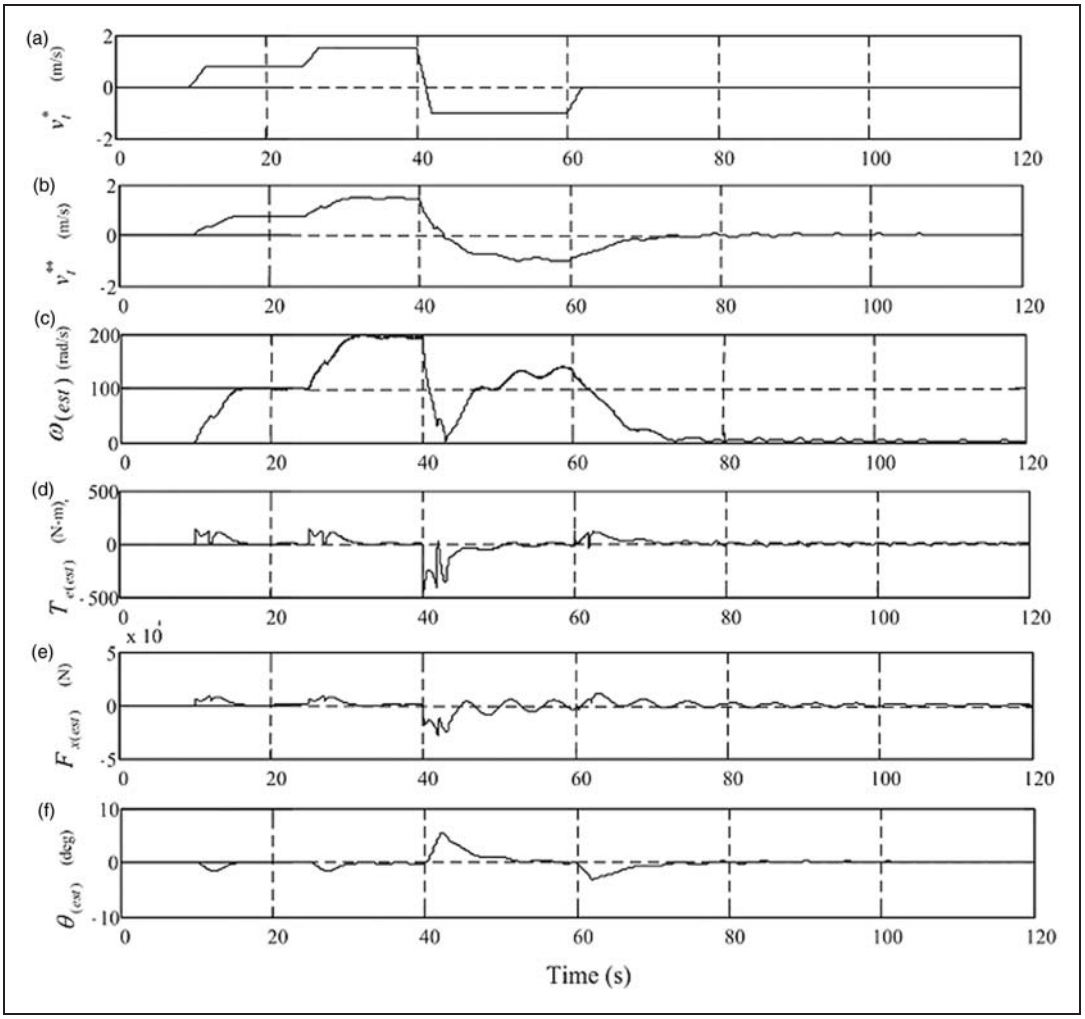

Figure 7. Performance of speed control scheme with anti-swing regulator (a) Trolley reference speed, (b) Modified trolley reference speed, (c) Estimated motor speed, (d) Estimated electrical torque, (e) Estimated forward drive force, and (f) Estimated swing angle.

measurement of electrical variables of trolley's motor drive is presented. In this method, the voltage and current of the induction motor is measured, then using these values, the electrical torque and motor speed are estimated, and then the amounts of adhesive force and swing angle are estimated.

This method is based on mathematical analysis and modeling, and estimation methods in dynamic situations have been used. It was shown that the estimated swing angle over different operational situations (i.e. start up, acceleration, and reversing movement direction, breaking and stopping) follows the actual swing angle, accurately, and the anti-swing system has damped the oscillations.

In this method, except in low price voltage and current sensors, there is no need for any more sensors.

To analyze the performance of the estimator system, the speed controller and the anti-swing regulator, the whole system is simulated and its proper performance is verified over the various operation conditions.

As a future work it is possible to improve the method considering noise and disturbances which exist in industrial environments.

Funding

This research received no specific grant from any funding agency in the public, commercial, or not-for-profit sectors.

Notation

a_{my}	Component of acceleration in the direction of y axis
a_{mn},a_{mt}	Normal and tangent components of the suspended load comparative acceleration

$\bar{a}_m$	Load mass acceleration
F_{ad}	Adhesion force
$\hat{F}_{ad}$	Estimated adhesion force in the direction of x axis
F_θ	Generalized force in the generalized coordinate directions of θ
g	Gravity acceleration
$\bar{i},\bar{j}$	Unit vectors
i_{rd},i_{rq}	Rotor two-phase currents
i_s	Stator current
i_{sA}, i_{sB}, i_{sC}	Stator three-phase currents
i_{sD},i_{sQ}	Stator two-phase currents
J	Moment of inertia
K_d	Damping coefficient
l	Suspending rope length
L_m	Magnetization inductance
L_r	Rotor inductance
L_s	Stator inductance
m	Load mass
M_t	Trolley mass
n,t	Normal and tangent axis
p	Number of poles/2
r	Trolley wheel radius
R_r	Rotor resistance
R_S	Stator resistance
T	Rope tension
T_e	Electrical torque
T_l	Load torque
T_x,T_y	Cartesian components of the rope tension
V_{rd},V_{rq}	Rotor two-phase voltages
V_{sA}, V_{sB}, V_{sC}	Stator three-phase voltages
v_s	Stator voltage
V_{sD}, V_{sQ}	Stator two-phase voltages
v_t	Actual trolley speed
v_t^*	Desirable speed reference
v_t^{**}	Modified speed reference
x, y	Cartesian components of the trolley (rope holder point)
x_m,y_m	Cartesian components of the suspended load
$\ddot{x}_m$	x- axis suspended load acceleration
α	Gear reduction ratio
θ	Load swing angle
$\hat{\theta}$	Estimated load swing angle
ψ_{sD},ψ_{sQ}	Stator two-phase fluxes
ψ_{rd},ψ_{rq}	Rotor two-phase fluxes
ω	Motor electrical speed

Crane parameters

20,000 (Kg)	(m) Load mass
18,300 (Kg)	(Mt) Trolley mass
10 (m)	(l) Rope length
1/100	(α) Gear reduction ratio
0.25 (m)	(r) Trolley wheels radius

References

Abdel-Rahman EM, Nayfeh AH and Masoud ZN (2003) Dynamics and control of cranes: A review. *Journal of Vibration and Control* 9(7): 863–908.

Cao L and Liu L (2011), Adaptive fuzzy sliding mode method-based position and anti-swing control for overhead cranes. In *Proceedings of Third International Conference on Measuring Technology and Mechatronics Automation*, Shanghai, People's Republic of China, Jan. 6–7, pp. 335–338.

Chang Y (2007) Adaptive fuzzy controller of the overhead cranes with nonlinear disturbance. *IEEE Transactions on Industrial Informatics* 3(2): 164–172.

Chwa D (2009) Nonlinear tracking control of 3-D overhead cranes against the initial swing angle and the variation of payload weight. *IEEE Transactions on Control Systems Technology* 17(4): 876–883.

Deng M, Wen S and Inoue A (2012) Sensorless anti-swing robust nonlinear control for travelling crane systems using SVR with generalized Gaussian function and robust right coprime factorization. *Transactions of the Society of Instrument and Control Engineers* 47(9): 366–373.

Ebeid AM, Moustafa KA and Emara-Shabaik H (1992) Electromechanical modeling of overhead cranes. *International Journal of Systems Science* 23(12): 2155–2169.

Ebrahimi M, Ghayour M, Madani SM and Khoobroo A (2011) Swing angle estimation for anti-sway overhead crane control using load cell. *International Journal of Control, Automation, and Systems* 9(2): 301–309.

Garrido S, Abderrahim M, Gimenez A, Diez R and Balaguer C (2008) Anti-swinging input shaping control of an automatic construction crane. *IEEE Transactions on Automation Science and Engineering* 5(3): 549–557.

Kaneko T, Mine H and Ohishi K (2009) Anti sway crane control based on sway angle observer with sensor-delay correction. *IEEJ Transactions on Industry Applications* 129(6): 555–563.

Kim YS, Seo HS and Sul SK (2001) A new anti- sway control scheme for trolley crane system. In *Proceedings of IEEE Conference on Industry Applications*, Chicago, IL, USA, 30 September– 4 October 2001, vol.1, pp. 548–552.

Kim YS, Hong KS and Sul SK (2004) Anti-sway control of container cranes: inclinometer, observer, and state feedback. *International Journal of Control, Automation, and Systems* 2(4): 435–449.

Liu Y, Yi J, Zhao D and Wang W (2004) Swing-free transporting of two-dimensional overhead crane using sliding mode fuzzy control. In *Proceedings of IEEE American Conference*, Boston, MA, June 30–July 2, vol. 2, pp. 1764–1769.

Moustafa KA and Ebeid AM (1988) Nonlinear modeling and control of overhead crane load sway. *ASME Transactions, Journal of Dynamic Systems, Measurements and Control* 110(3): 266–271.

Noakes MW and Jansen JF (1992) Generalized inputs for damped-vibration control of suspended payloads. *Elsevier Robotics and Autonomous Systems* 10(2–3): 199–205.

Pannil P, Smerpitak K, La-orlao V and Trisuwannawat T (2010) Load swing control of an overhead crane. In *Proceedings of International Conference on Control, Automation and Systems*, Gyeonggi-do, Korea, Oct. 27–30, pp. 1926–1929.

Park BJ, Hong KS and Huh CD, (2000) Time-efficient input shaping control of container crane systems. In *Proceedings of the 2000 IEEE International Conference on Control Application*, Anchorage, AK, 25–27 September 2000, pp. 80–85.

Park MS, Chwa D and Hong SK (2008) Anti-sway tracking control of overhead cranes with system uncertainty and actuator nonlinearity using an adaptive fuzzy sliding-mode control. *IEEE Transactions on Industrial Electronics* 55(11): 3972–3984.

Piazzi A and Visioli A (2002) Optimal dynamic-inversion-based control of an overhead crane. In *Proceedings of IEE Control and Application,* Trieste, Italy, September 2002, vol. 149, pp. 405–411.

Rushmer MW, Ruddy TA, Brukalo K and Ritter AM (1995) Electronic anti-sway control. *US Patent 5443566*.

Saeidi H, Naraghi M and Raie AA (2012) A neural network self tuner based on input shapers behavior for anti sway system of gantry cranes. *Journal of Vibration and Control* 1–14.

Sano H, Sato K, Ohishi K and Miyazaki T (2012) Robust design of vibration suppression control system for crane using sway angle observer considering friction disturbance. *IEEJ Transactions on Industry Applications* 132(3): 357–365.

Siemens (1999) Drive and control components for hoisting gear. *Siemens, Catalog HE 1*.

Solihin ML (2009) Sensorless anti-swing control of automatic gantry crane using dynamic recurrent neural network-based soft sensor. *International Journal of Intelligent Systems Technologies and Applications* 6(1–2): 112–127.

Solihin ML, Wahyudi M and Legowo A (2010) Fuzzy-tuned PID anti-swing control of automatic gantry crane. *Journal of Vibration and Control* 16(1): 127–145.

Sorensen KL (2005) A combined feedback and command shaping controller for improving positioning and reducing cable sway in cranes. M.Sc. Thesis, School of Mechanical Engineering Georgia Institute of Technology, GA.

Trabia MB, Renno JM and Moustafa KAF (2008) Generalized design of an anti-swing fuzzy logic controller for an overhead crane with hoist. *Journal of Vibration and Control* 14(3): 319–346.

Tsai NC, Chen DC, Shih LW and Chiang CW (2011) Model reduction and composite control for overhead hoist transport system by singular perturbation technique. *Journal of Vibration and Control*, 18(8): 1018–1095.

Umez-Eronini EI (1998) *System Dynamics and Control*. CL-Engineering.

Vas P (1998) *Sensorless Vector and Direct Torque Control*. Oxford, UK: Oxford University Press.

Wen S, Deng M and Wang D (2011) Operator-based robust nonlinear control for a crane system with constraint inputs. In *Proceedings of 30th Chinese Control Conference (CCC),* Yantai, People's Republic of China, July 22–24, pp. 6109–6114.

Yu W and Li X (2010) Anti-swing control for an overhead crane with intelligent compensation. In *Proceedings of 3rd International Symposium on Resilient Control Systems (ISRCS),* Idaho Falls, ID, Aug. 10–12, pp. 85–90.

Zhong B and Zhan R (2012) Load's damping swing by trolley's driving force control for overhead or gantry crane. *Advanced Materials Research* 346: 875–881.